



A proposal on how to perform the VBF $H \rightarrow c\bar{c}$ search at the CMS experiment

Marco Cecca
University of Bari, Italy

Abstract

The goal of this measurement is to study the kinematic variables of the jets produced by the Higgs boson decaying into c -quarks predicted by the Standard Model (SM), after it has been produced through the Vector Boson Fusion VBF . For this purpose a root-file containing several variables associated to the events generated with MadGraph5_aMC@NLO and those reconstructed through Geant4 was used. After a kinematic analysis of the event, a score was finally defined to assess whether the reconstructed jets came from the hadronization of the c -quark, so that the invariant mass of the Higgs boson could be correctly reconstructed.

Contents

1	Introduction	2
1.1	Higgs boson production and decay mechanisms	2
2	CMS Experiment	5
2.1	Overview of the structure	5
2.2	The inner tracker	5
2.3	The calorimeters	6
2.4	The superconducting Magnet & Muon detection	6
3	Signal properties	7
3.1	Vector Boson Fusion Mode	7
3.2	Kinematics of the Higgs decay products	7
4	Identification of jets	11
4.1	Jet reconstruction	11
4.2	Identification of heavy-flavour jets	11
4.3	The c -tagging and ParticleNet	12
5	Conclusion	13

1 Introduction

1.1 Higgs boson production and decay mechanisms

In the SM the Higgs mechanism explains the electroweak symmetry breaking and allows electroweak gauge bosons to acquire mass. The mechanism predicts the existence of a Higgs scalar boson, and its observation was one of the main goals of the LHC physics program.

At the LHC, a standard model Higgs boson can be produced through a variety of different mechanisms. The expected production cross sections as a function of the Higgs boson mass predict that after the gluon-gluon fusion mechanism (ggF), the second largest Higgs boson production cross section is expected to be the vector boson fusion (VBF) mechanism [7][6]. Furthermore, for a SM Higgs boson with a mass $m_H < 135 \text{ GeV}^1$, the expected dominant decay mode is to a b -quark pair ($b\bar{b}$). In particular, this work presents the search for a SM Higgs boson in the VBF production mode, followed by a $c\bar{c}$ decay, which occurred with less than 3% of total channels decay [7][6]. The associated Feynman diagrams are shown in *Figure 1*.

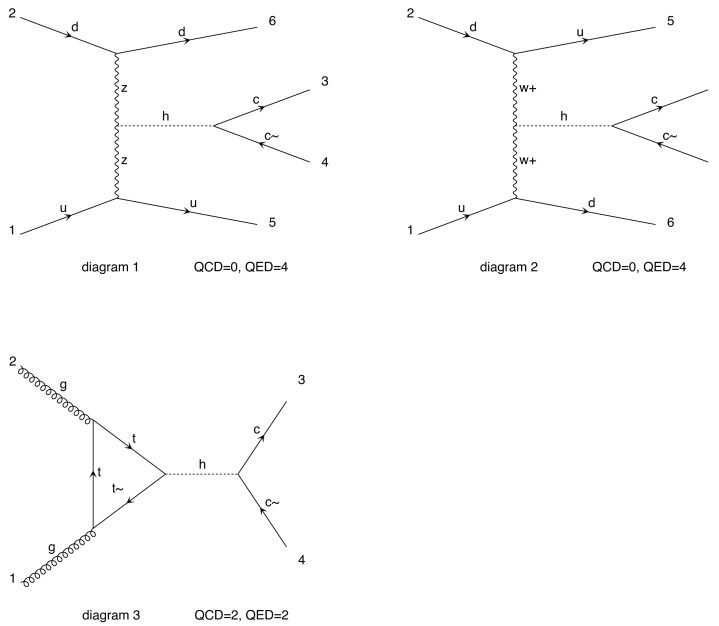


Figure 1: Main leading order Feynman diagrams contributing to the Higgs boson production in gluon-gluon fusion ggF (bottom) and Vector boson fusion VBF (top), both followed by a c -quark decay. All the diagrams were obtained using MadGraph5_aMC@NLO.

Instead in *Figure 2* (left) the cross sections for the production of a SM Higgs boson as a function of \sqrt{s} , the center of mass energy, for pp collisions is represented and in *Figure 2* (right) the branching ratios for the main decays of the SM Higgs boson near $m_H = 125 \text{ GeV}$ is shown.

¹From this point on, the use of natural units will be implied, with $\text{GeV}/c^2 = \text{GeV}$ for masses and $\text{GeV}/c = \text{GeV}$ for momentum.

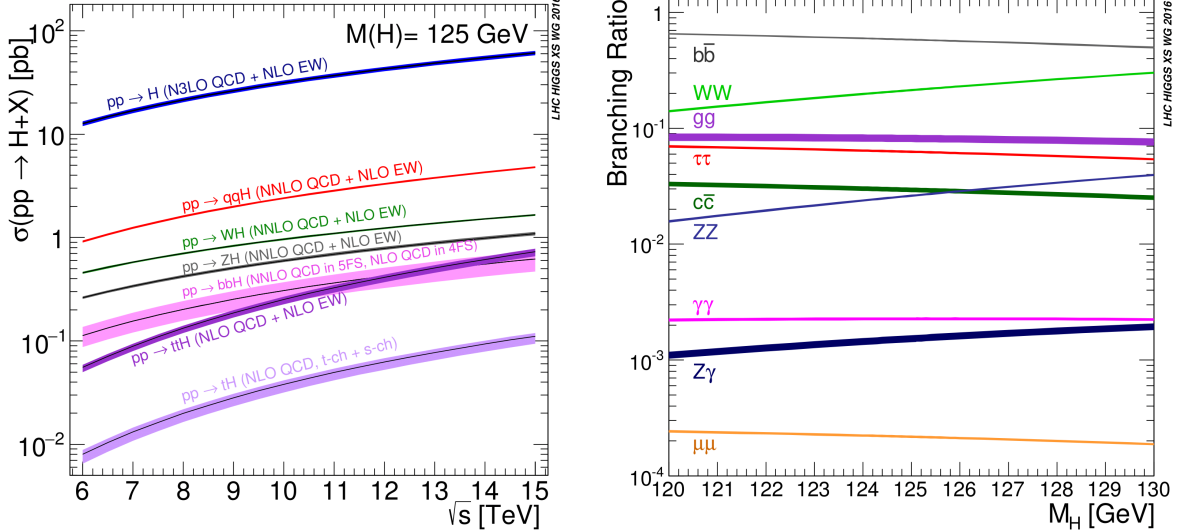


Figure 2: (Left) The SM Higgs boson production cross sections as a function of the center of mass energy, \sqrt{s} , for pp collisions. The VBF process is indicated here as qgH . The theoretical uncertainties are indicated as bands [8]. (Right) The branching ratios for the main decays of the SM Higgs boson near $m_H = 125\text{GeV}$. The theoretical uncertainties are indicated as bands [8].

Assuming now an integrated luminosity of 100 fb^{-1} and a Higgs boson mass of $m_H = 125.09\text{ GeV}$, we can estimate the expected number of events ², according to the SM, as the energy of the center of mass \sqrt{s} varies, for both ggF and VBF, using the corresponding cross sections [7]. Finally, considering a branching ratio of 2.89×10^{-2} [7] for the Higgs decay in a $c\bar{c}$ pair, we can obtain the final number of events of interest. These results are summarized in the *Table 1* and *Table 2*.

\sqrt{s} [TeV]	Cross Section [pb]	# Tot Events of VBF production	# Tot Events of the decay $H \rightarrow c\bar{c}$
7.0	1.241	1.2E+05	3.6E+03
8.0	1.601	1.6E+05	4.6E+03
13.0	3.782	3.8E+05	1.1E+04

Table 1: Vector boson fusion production VBF: an integrated luminosity of 100 fb^{-1} and a Higgs boson mass of $m_H = 125.09\text{ GeV}$ was assumed. The cross sections and the branching ratio value have been taken from Ref.[7].

\sqrt{s} [TeV]	Cross Section [pb]	# Tot Events of ggF production	# Tot Events of the decay $H \rightarrow c\bar{c}$
7.0	16.83	1.7E+06	4.9E+04
8.0	21.39	2.1E+06	6.2E+04
13.0	48.51	4.9E+06	1.4E+05

Table 2: Gluon Fusion production ggF: an integrated luminosity of 100 fb^{-1} and a Higgs boson mass of $m_H = 125.09\text{ GeV}$ was assumed. The cross sections and the branching ratio value have been taken from Ref.[7].

²The expected number of events is obtained from $N_{Events} = \sigma \times L_{int}$

As can be seen in both cases, ggF and VBF, the number of expected events increases as the energy of the center of mass increases. This is because the expected number of events of a given process in a collider is directly proportional to the integrated luminosity and to the cross section of the selected process, which increases as the energy of the center of mass increases.

The dominant process at LHC in the production of the Higgs boson is through the gluon-gluon fusion (ggF): the two gluons combine to form a loop of virtual quarks. Since the coupling of particles to the Higgs boson is proportional to their mass, this process is more likely for heavy particles (virtual top and bottom quarks) (*Figure 1-bottom*).

The second most important production process is the vector boson fusion (VBF): when two fermions collide is that the two exchange a virtual W or Z boson, which emits a Higgs boson. The colliding fermions do not need to be the same type. It has a very distinctive topology because in addition to the Higgs boson, we expect to have two light quarks with large pseudorapidity (*Figure 1-top*). This allows us to identify through the detector system in the final state, two jets generated by the hadronization of quarks, emitted in the forward and backward direction of the beam

In particular, it can be seen that the cross sections of the two processes differ by as much as an order of magnitude. This difference in the cross section magnitude is related to the coupling strength and the partonic distribution functions (PDF) in the proton at the LHC energy scale. The Higgs boson couples to particles with mass, and the strength of this coupling is proportional to the mass of the interacting particle: in ggF, the Higgs boson is produced via a loop of virtual heavy quarks, further enhancing the coupling due to their large masses. In VBF, the interaction involves weak vector bosons (W or Z bosons) that have relatively smaller masses, leading to a weaker coupling to the Higgs boson. Additionally, gluons have higher PDFs than quarks at the energy scales of the LHC, making ggF more likely due to the increased probability of finding gluons within the colliding protons.

In the end, after the Higgs boson production, it has many different processes through which it can decay [7]. Each of these possible processes has its own probability, expressed as the branching ratio, the fraction of the total number decays that follows that process. The SM predicts these branching ratios as a function of the Higgs mass. One way that the Higgs can decay is by splitting into a fermion–antifermion pair: in particular, the decay in $c\bar{c}$, which happens only about 2.8% of the time, will be analyzed. In the end considering the production of the Higgs boson through the VBF and the subsequent $c\bar{c}$ decay, there will be an event characterized by four jets due to hadronization of the products of the decay and the hard scattering.

2 CMS Experiment

2.1 Overview of the structure

The Compact Muon Solenoid (CMS) experiment is a general-purpose particle physics detector built on the Large Hadron Collider (LHC) [3]. The goal of CMS experiment is to investigate a wide range of physics, including the search for the Higgs boson. The CMS detector is built around a huge solenoid magnet. This takes the form of a cylindrical coil of superconducting cable that generates a magnetic field of 4 teslas. It contains subsystems which are designed to measure the energy and momentum of photons, electrons, muons, and other products of the collisions. The innermost layer is a silicon-based tracker. Surrounding it is a scintillating crystal electromagnetic calorimeter, which is itself surrounded with a sampling calorimeter for hadrons. The tracker and the calorimetry are compact enough to fit inside the CMS solenoid. Outside the magnet are the large muon detectors, which are inside the return yoke of the magnet. A scheme of the apparatus is showed in *Figure 3*.

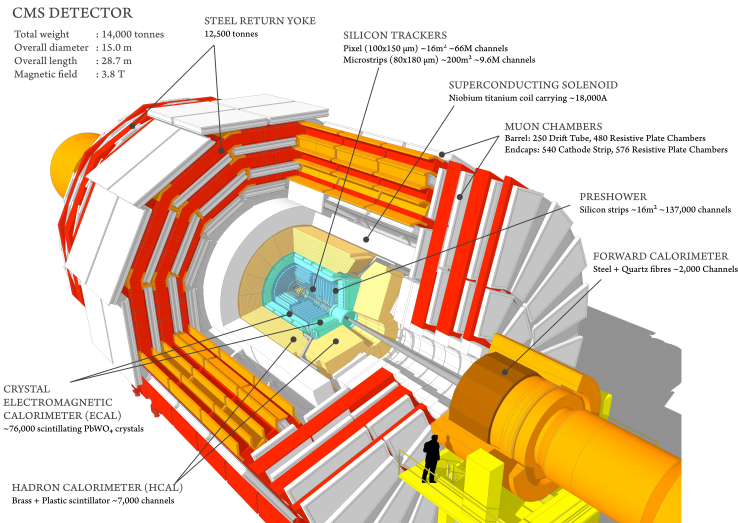


Figure 3: Scheme of the CMS detector and its main components [12]

2.2 The inner tracker

The tracker is the closest detector to the beamline, and is mainly responsible for reconstruction of tracks and vertices. The CMS tracking system is designed to reconstruct high-pT muons, isolated electrons and hadrons with high momentum resolution and an efficiency better than 98% in the range $|\eta| < 2.5$ and is made up of two sub-detectors. The first consists of three layers of silicon pixel detector, which is the innermost detector with the biggest granularity in order to handle the large multiplicities present in the area. Instead, the outer detector is made of ten layers of silicon microstrip detectors, which provide the required granularity and precision [9].

Accurate measurement of secondary vertices, and thus impact parameters, is required to study quark decays and additionally, detection of particle jets arising from c quark decays, *c-tagging*, is a very important tool for the search of the Higgs boson. At the state of the art the impact parameter resolution is ranging from $35\mu\text{m}$ to $75\mu\text{m}$ depending on the pseudorapidity range $|\eta| = [0, 2.5]$. Instead the transverse momentum resolution is between 2% and 6% depending on the range [9].

2.3 The calorimeters

Electrons, photons and hadrons will deposit their energies in the calorimeters allowing their energy to be measured. The first calorimeter layer or Electromagnetic Calorimeter (ECAL) is designed to measure the energies of electrons and photons with high precision. Strongly-interacting particles, hadrons, deposit most of their energy in the second layer, the hadron calorimeter (HCAL). Muon leptons deposit only a very small fraction of their energy in the calorimeters, and are detected by consulting also with tracking and muon detector subsystems. Neutrinos escape detection, but their presence can be inferred from an apparent energy imbalance in the interaction.

The ECAL is surrounded by a brass/scintillator sampling Hadron Calorimeter (HCAL) with coverage up to $|\eta| < 3.0$. It has an high granularity of $\Delta\phi \times \Delta\eta = 0.087 \times 0.087$ for $|\eta| < 1.6$ and for greater pseudorapidity regions $\Delta\phi \times \Delta\eta = 0.17 \times 0.17$. Instead the HCAL resolution in energy for single particle is $\sim \frac{70\%}{\sqrt{E}} \oplus 5\%$ (at $\eta = 0$) [5]. The HCAL [4] plays an essential role in the identification and measurement of missing transverse energy and quarks, gluons, and neutrinos by measuring the energy and direction of jets. The hadronic calorimeter is a hermetic sampling calorimeter consisting of several layers of brass absorber and plastic scintillator tiles, read out via wavelengthshifting fibres by hybrid photodiodes. This combination was determined to allow the maximum amount of absorbing material inside of the magnet coil.

The scintillation light is converted by wavelength-shifting (WLS) fibers embedded in the scintillator tiles and channelled to photodetectors via clear fibres. While most of the HCAL is contained inside the CMS magnet, there are several additional layers outside the magnet to detect particles from high energy showers. The depth of the HCLA ensures that hadronic showers are sampled with nearly 11 hadronic interaction lengths. This is needed to contain high-energy jets and accurate measurements of high-energy jets is important for searches for high mass SM Higgs boson.

There are also "forward" HCAL's installed at each end of the CMS detector which provide coverage up to a pseudorapidity η of 5.0 with a resolution of $\sigma/E = \frac{100\%}{\sqrt{E}} \oplus 5\%$ [5]. Wide rapidity coverage and accurate energy measurements are the main requirements of the hadron calorimetry system as several Higgs modes require good missing transverse energy measurements.

2.4 The superconducting Magnet & Muon detection

The central feature of the CMS design is a large superconducting solenoid magnet. It delivers an axial and uniform magnetic field of 3.8 T over a length of 12.5 m and a radius of 3.15 m. This radius is large enough to accommodate the tracker and both the ECAL and HCAL, minimizing the amount of material in front of the calorimeters. This feature eliminates the energy losses before the calorimeters caused by particles showering in the coil material and facilitates the link between tracks and calorimeter clusters.

As the name "Compact Muon Solenoid" suggests, detecting muons is one of CMS's most important tasks [10]. Because muons can penetrate several metres of iron without interacting, unlike most particles they are not stopped by any of CMS's calorimeters. Therefore, chambers to detect muons are placed at the very edge of the experiment where they are the only particles likely to register a signal.

3 Signal properties

3.1 Vector Boson Fusion Mode

As mentioned earlier in this work, the decay of the Higgs boson in $c\bar{c}$ was investigated after its production by VBF. Infact the observation of the SM Higgs boson decaying to $c\bar{c}$ pairs is not imaginable considering the ggF in proton collisions ³, instead in the VBF production context it can be pursued thanks to the kinematic properties of the VBF process. The prominent feature of the searched signal is the presence of four energetic hadronic jets generated in the final state (*Figure 1 - top*). Two jets are expected to originate from a light-quark pair (u,d-type), that are typically two valence quarks from each of the colliding protons scattered away from the beam line and two additional jets are expected from the Higgs boson decay to $c\bar{c}$. Furthermore, the partons interact through the weak force, so there is no exchange of color charges between the initial e final state at leading order: very little additional QCD radiation and hadronic activity is expected.

3.2 Kinematics of the Higgs decay products

In the first place, the number of generated and reconstructed jets per event was studied. As mentioned above we expect four jets generated per event due to the hadronization of two light quarks and two c-quarks from the higgs. This distribution is shown in *Figure 4*.

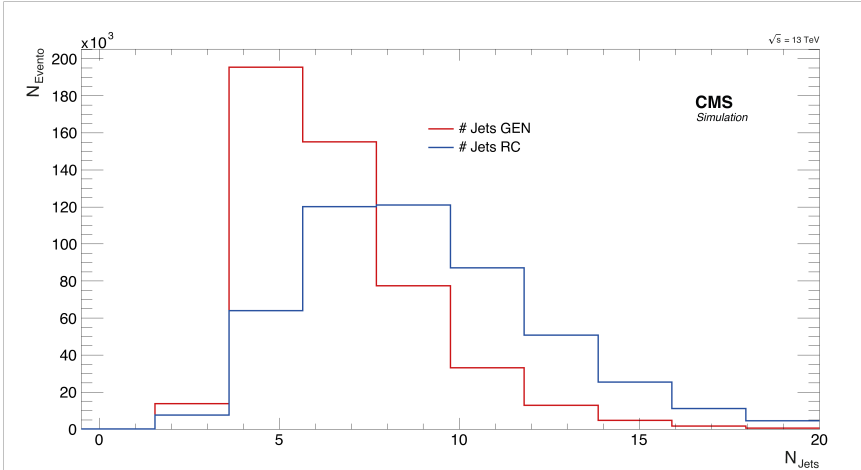


Figure 4: Distribution of the number of jets generated and reconstructed per event.

As can be seen both generated and reconstructed jets per event are greater than four. Specifically, for the generated there are an average of six jets per event, while for the reconstructed there are an average of fifteen jets. This can be explained by considering that the simulation of the generated event also includes the eventual initial and final state radiation, which upon hadronization generates other jets. In addition, both at the level of generated and reconstructed, jet reconstruction algorithms have limited efficiency.

The plots of the kinematic variables distributions, such as the transverse momentum p_T , the psedorapidity η and the azimuthal angle ϕ , are shown below both for the generated jets and the reconstructed ones. More precisely, the reconstructed jets were divided into: the

³Because of the irriducible QCD background, which is order of magnitude larger than the Higgs production cross section [13]

jets associated with the corresponding generated jets related to the Higgs decay, and the remaining ones. This association between reconstructed and generated was made by considering a geometric association: a reconstructed jet was considered to have come from the Higgs decay if the corresponding generated jet was distant less than 0.5 from it, in $\eta - \phi$ space:

$$DR = \sqrt{(\phi_{JetGEN} - \phi_{JetRC})^2 + (\eta_{JetGEN} - \eta_{JetRC})^2} < 0.5 \quad (1)$$

From the plots *Figure 5-6-7* it is observed that the distributions of the various observables associated with the jets are similar between the generated and reconstructed level. However, the generated particles are just points in phase space with certain information, while the variables associated with the reconstructed particles are affected by their interaction with the simulated detectors, the response of the latter, and finally by the reconstruction algorithms (tracking, clustering, and jet reconstruction). Nevertheless it can be seen that the reconstruction of the jets from Higgs had a high efficiency as there were almost as many jets reconstructed as generated.

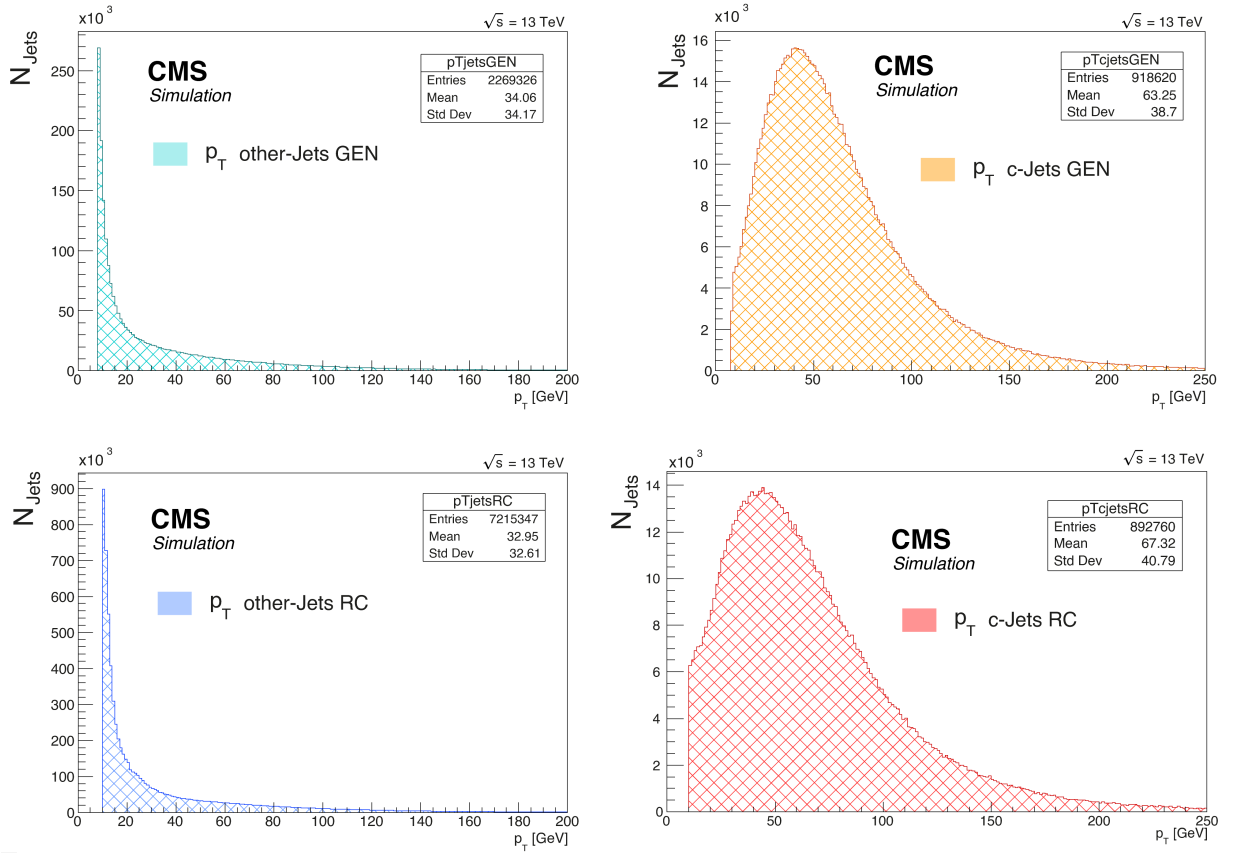


Figure 5: Transverse momentum p_T of: generated GEN jets from hard scattering (top-left), generated GEN jets from Higgs decay (top-right), reconstructed RC jets from hard scattering (bottom-left) and reconstructed RC jets associated to generated from Higgs decay (bottom-right).

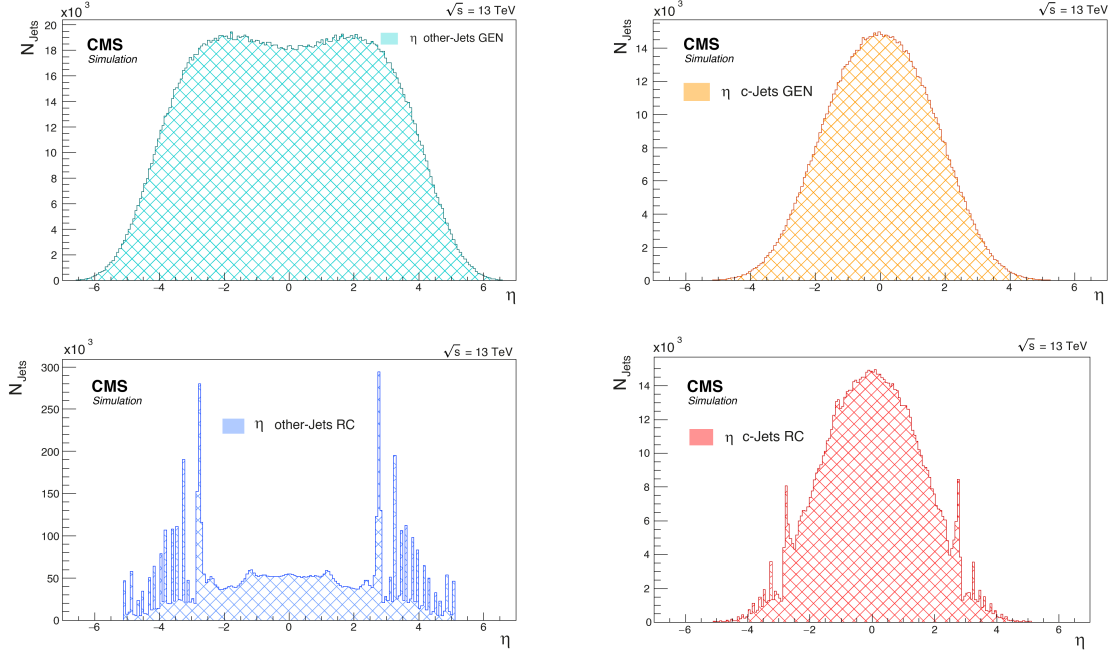


Figure 6: Pseudorapidity η of: generated GEN jets from hard scattering (top-left), generated GEN jets from Higgs decay (top-right), reconstructed RC jets from hard scattering (bottom-left) and reconstructed RC jets associated to generated from Higgs decay (bottom-right).

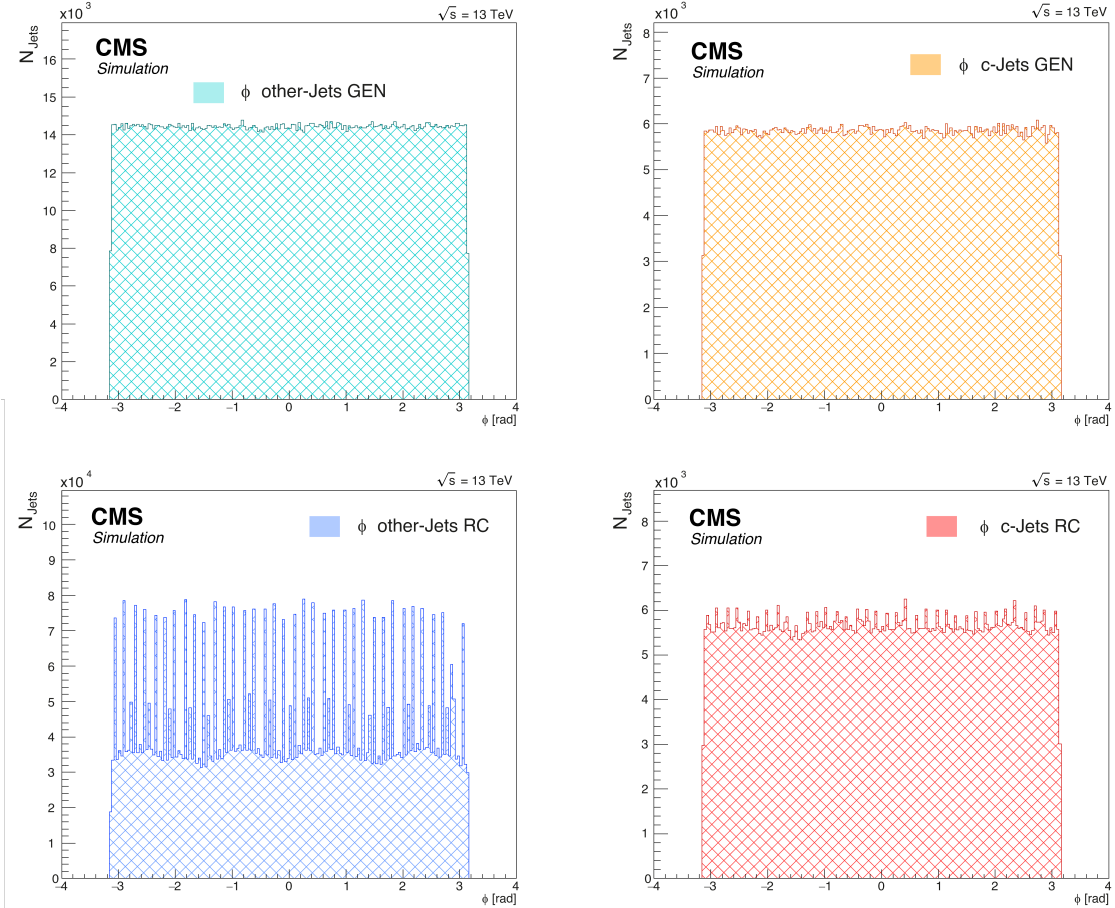


Figure 7: Azimuthal angle ϕ of: generated GEN jets from hard scattering (top-left), generated GEN jets from Higgs decay (top-right), reconstructed RC jets from hard scattering (bottom-left) and reconstructed RC jets associated to generated from Higgs decay (bottom-right).

First of all, it can be observed in *Figure 6* how the jets produced in the hard scattering are roughly in the forward and backward directions relative to the beam direction with large pseudorapidity. Instead, the c-jets originated from Higgs are distributed more in the central regions of the detector. The differences in shape between the reconstructed and generated jets distribution could be related to the reconstruction algorithm efficiency and to detector geometry implemented on GEANT4. For example, the inner tracker layout at CMS has an extension to $|\eta| \sim 2.5$ [9], in particular the two End Caps (HE), has a coverage of $1.3 < |\eta| < 3.0$ [4]. Therefore, although there are jets generated with even greater pseudorapidity, they are not reconstructed correctly, or at all, by the simulation. Furthermore both the transverse momentum and the pseudorapidity are extrapolated from the curvature measurement and therefore uncertainty on radius is propagated.

Whereas, observing the transverse moment distribution *Figure 5 (left)*, one can see that the jets generated and reconstructed, coming from hard scattering, have a low p_T as expected from the pseudorapidity distribution. Additionally, it is possible to further investigate the distribution of the transverse momentum of the reconstructed jets associated with the generated from the Higg in *Figure 5 (right)*. To do this I exploit the CvsAll score (introduced later in the *Section 4.3*), which gives information about the probability that the jet is c-tagged. Comparing this score with the distribution of p_T for the reconstructed jets related to Higgs, one can see in the *Figure 8* how there is a major thickening of low p_T jets with a low CvsAll value and another thickening around $50 - 60\text{GeV}$ with a high CvsAll value. This perfectly mirrors the distribution of the CvsAll value presented later.

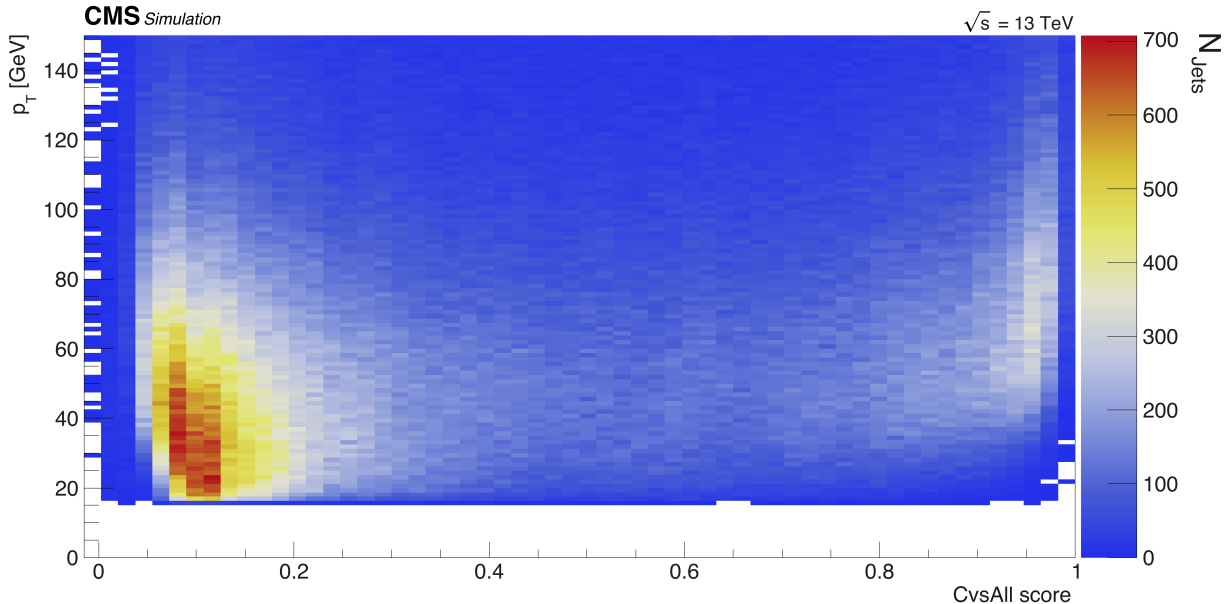


Figure 8: Two dimensional plot that shows the relation between the CvsAll score and the p_T value of the reconstructed jet related to the generated ones from the Higgs decay products.

4 Identification of jets

4.1 Jet reconstruction

Since gluons and quarks could not exist into free state, they fragment into hadrons resulting into a jet of particles depositing energy in the detectors. There is a wide range of algorithms for jet reconstruction as cone-based algorithms or a k_T algorithm⁴. The latest jets clustering algorithms use all the informations available from all detectors and subdetectors to measure the energy and the momentum of each particle which leaves a signal: this approach, extensively used in the CMS experiment, is called particle flow.

4.2 Identification of heavy-flavour jets

Algorithms for heavy flavour jet identification use variables connected to the properties of heavy flavour hadrons present in jets resulting from the radiation and hadronization of b or c quarks. For instance, the life time of hadrons containing c hadrons is 1 ps or less. This leads to typical displacements of a few mm, depending on their momentum, thus giving rise to displaced tracks from which a secondary vertex (SV) may be reconstructed, as shown in *Figure 9*. The displacement of tracks with respect to the primary vertex is characterized by their impact parameter, which is defined as the distance between the primary vertex and the tracks at their points of closest approach. For this reason it is important that the tracking system has high resolution to reconstruct tracks and recognize primary and secondary vertices.

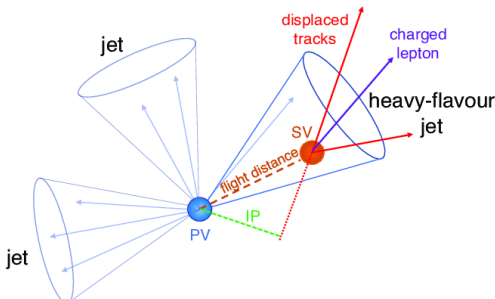


Figure 9: Illustration of a heavy-flavour jet with a secondary vertex (SV) from the decay of a b or c hadron resulting in charged particle tracks (including possibly a soft lepton) that are displaced with respect to the primary interaction vertex (PV), and hence with a large impact parameter (IP) value. [1]

In addition, c quarks have a larger mass and harder fragmentation compared to the light quarks and massless gluons. As a result, the decay products of the heavy-flavour hadron have, on average, a larger p_T relative to the jet axis than the other jet constituents. In approximately 10% [1] of the cases, a muon or electron is present in the decay chain of a heavy c hadron. Hence, a part from the properties of the reconstructed secondary vertex or displaced tracks, the presence of charged leptons is also exploited for heavy-flavour jet identification techniques.

⁴In particular in this analysis a *anti* – k_T was used, constructing AK4Puppi (Pileup Per Particle Identification) jets. It essentially behaves like an idealised cone algorithm: in fact there is also the radius parameter R, which can be identified as the radius of the reconstructed idealised cone and there is a new parameter added p used to govern the power of the energy. The p parameter is negative and from this value comes the name of "anti-kt" [2]. This particular algorithm is dominated by high p_T and prefers to cluster hard particles first.

4.3 The c-tagging and ParticleNet

The algorithms which attempt to reconstruct these properties in terms of heavy quark identification are called *c-tagging* algorithms. The main idea of an algorithm is to associate a floating point number to a jet, where conventionally large values are associated to a jet originating from a heavy hadron while small values are associated to jets originating from light partons (uds). This is critical for the analysis of the Higgs boson decay in $c\bar{c}$, as it is necessary, once the jets are reconstructed, to identify which of them come from hadronization of the decay products. In addition these algorithms can be classify according to the set of variables used to tag the hadron such as the value of the impact parameter or the values related to a reconstructed secondary vertex.

In this analysis the *ParticleNet* [11] algorithm was used: the jets are treated as an un ordered set of particles, like a "particle cloud" in the ϕ - η space and using Dynamic Graph Convolutional Neural Network (DGCNN), the algorithm associates each jet with the probability that it was initialized by uds-type quarks, c quarks or gluons. By combining these probability values, a *CvsAll*⁵ discriminator defined as:

$$CvsAll = \frac{p(c)}{p(c) + p(u) + p(d) + p(s) + p(g)} \quad (2)$$

used to separate the c-jets from the rest (uds). Specifically, by comparing the value of CvsAll associated with the reconstructed jets from the Higgs decay with the remaining reconstructed jets, it was possible to define a threshold value for CvsAll above which the jet could be considered to have been produced from c-quark hadronization. This comparison is shown in *Figure 10*.

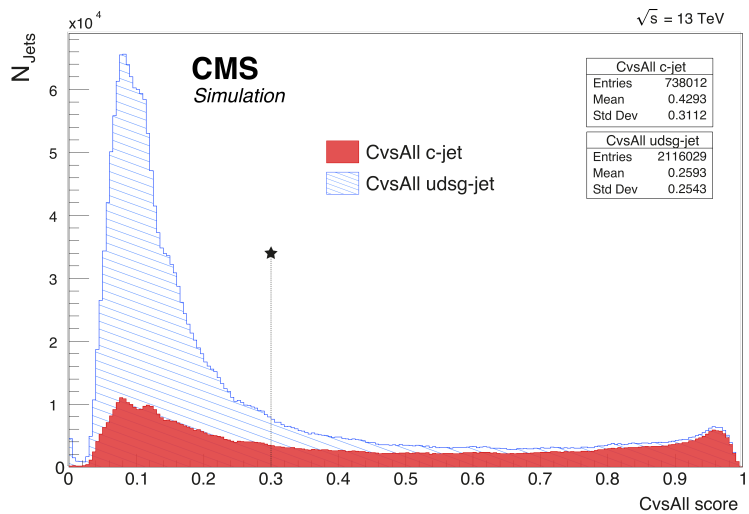


Figure 10: CvsAll Score comparison between jets reconstructed from Higgs decay in $c\bar{c}$ and the other light-quark jets. As can be seen, the CvsAll value associated to udsg-quark jets is mostly before the 0.3 (it is marked by a dotted line).

⁵In the actual analysis the individual probabilities $p(u)$ $p(d)$ $p(s)$ are merged together in a single value $p(uds)$

As can been seen from the plot above, the CvsAll score has an high discriminant power and a reasonable threshold value for CvsAll score can be set at 0.3. In fact, by making this cut, most of the reconstructed jets that do not come from the Higgs decay in $c\bar{c}$ are excluded: the blue region in *Figure 10* is the distribution of the reconstructed Jets that have not been associated with a generated one. At the end all the reconstructed couple of jets that satisfy the threshold value and that have been associated with the reconstructed, are used to obtain the inviariant mass of Higgs Boson *Figure 11*.

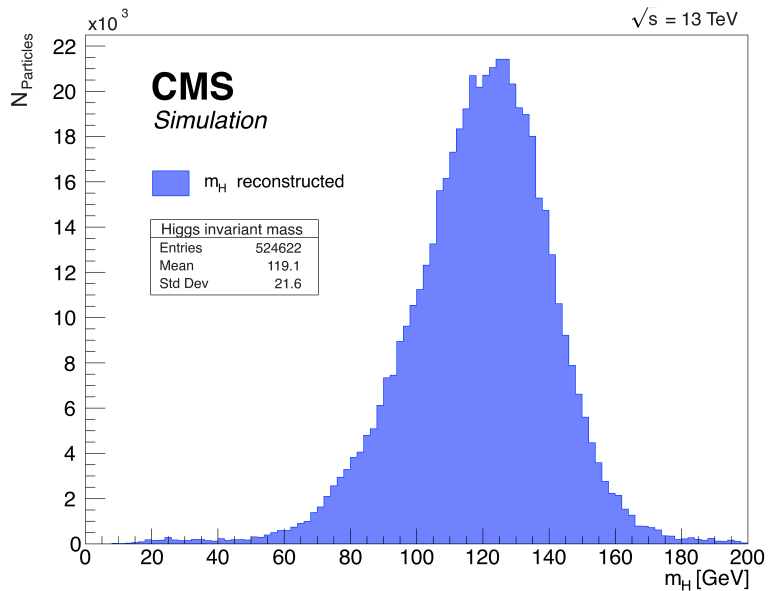


Figure 11: Dijet mass distribution for simulated signal events after the selection criteria peaks at Higgs boson mass.

5 Conclusion

A search for the standard model Higgs boson produced in the vector boson fusion production channel with decay to charm quarks has been performed in a data simulated sample of pp collisions in CMS at $\sqrt{s} = 13 \text{ TeV}$. The events are been reconstructed using the particle-flow algorithm. Instead, the Higgs jets are been reconstructed with the $anti - k_T$ algorithm with radius $R = 0.4$ and c-tagged combining several probabilities obtained from the ParticleNet algorithm. Through this descriminator it was possible to select the jets useful for the reconstruction of the Higgs invariant mass distribution presented in *Figure 11*. What was not taken into account in this analysis is the presence of background events. In particular, one can think of isolating the signal events by exploiting the characteristic topology of production by VBF of the Higgs, so as to distinguish it from production by gluon-gluon fusion and subsequently from the QCD background. For the latter in particular, one can think of proceeding with a multivariate analysis of the kinematic variables associated with the signal and background, possibly including machine learning algorithms, in order to efficiently distinguish signal events to be later compared with experimental data. For data taking will therefore require, in addition to properly calibrated and efficient calorimeters and tracking systems as described in the Section 2, an efficient trigger system and subsequent proper interpretation of the data in order to handle multiple interactions and pileup.

References

- [1] W. Adam A.M. Sirunyan, A. Tumasyan. Identification of heavy-flavour jets with the cms detector in pp collisions at 13 tev. *Journal of Instrumentation*, 13(05):P05011, may 2018.
- [2] Matteo Cacciari, Gavin P. Salam, and Gregory Soyez. The anti-kt jet clustering algorithm. *Journal of High Energy Physics*, 2008(04):063, apr 2008.
- [3] CMS Collaboration. The CMS experiment at the CERN LHC. The Compact Muon Solenoid experiment. *JINST*, 3:S08004, 2008. Also published by CERN Geneva in 2010.
- [4] CMS Collaboration. CMS Technical Design Report for the Phase 1 Upgrade of the Hadron Calorimeter. Technical report, CERN, 2012.
- [5] CSM. *The CMS hadron calorimeter project: Technical Design Report*. Technical design report. CMS. CERN, Geneva, 1997.
- [6] LHC Higgs Cross Section Working Group. Handbook of lhc higgs cross sections: 2. differential distributions. <http://cds.cern.ch/record/1416519>, 2012.
- [7] LHC Higgs Working Group. Higgs cross-section and branching ratios. <https://twiki.cern.ch/twiki/bin/view/LHCPhysics/LHCHWG>.
- [8] Particle Data Group and Workman. Review of Particle Physics. *Progress of Theoretical and Experimental Physics*, 2022(8):083C01, 08 2022.
- [9] V. Karimäki. The CMS tracker system project: Technical Design Report. 1997.
- [10] J. G. Layter. *The CMS muon project: Technical Design Report*. Technical design report. CMS. CERN, Geneva, 1997.
- [11] Huilin Qu and Loukas Gouskos. Jet tagging via particle clouds. *Physical Review D*, 101(5), mar 2020.
- [12] Tai Sakuma. 3D SketchUp images of the CMS detector (120918), 2016.
- [13] James Stirling. PARTON LUMINOSITY AND CROSS SECTION PLOTS. <http://www.hep.ph.ic.ac.uk/~wstirlin/plots/plots.html>.